Rough 1D photonic crystals: A transfer matrix approach

Leandro L. Missoni [a], Guillermo P. Ortiz [b,*], María Luz Martínez Ricci [a], Victor J. Toranzos [d], W. Luis Mochán [e]

[a] *Instituto de Química Física de los Materiales, Medioambiente y Energía (INQUIMAE-CONICET), DQIAQF, Facultad de Ciencias Exactas y Naturales, Universidad de Buenos Aires, Pabellón II, Ciudad Universitaria, C1428EHA, Buenos Aires, Argentina*

[b] *Departamento de Física, Facultad de Ciencias Exactas Naturales y Agrimensura, Universidad Nacional del Nordeste, Corrientes, Argentina*

[d] *Departamento de Ingenieria, Facultad de Ciencias Exactas Naturales y Agrimensura, Universidad Nacional del Nordeste, Corrientes, Argentina*

[e] *Instituto de Ciencias Físicas, Universidad Nacional Autónoma de México, Av. Universidad s/n, Col. Chamilpa, 62210, Cuernavaca, Morelos, Mexico*

ARTICLE INFO

ABSTRACT

Interfacial roughness is prevalent in 1D photonic crystals and other layered structures, but is not generally accounted for in their design nor the analysis of their optical properties due to a lack of simple theoretical approaches. We present a transfer matrix formalism to incorporate the effects of interfacial roughness in the optical properties of stratified systems such as 1D photonic crystals and apply it to calculate the optical response of some nanoporous anodic alumina and porous silicon structures. We have validated our formalism by comparing our results to some experiments.

1. Introduction

Nanomaterials have gained a lot of interest in diverse fields of active research due to their unique properties. Manipulation of their composition, characteristic size, and shape allows tuning their optical, electrical and chemical properties, which might differ substantially from those of their components. In the last decades, the variety of synthesis procedures for nanomaterials has increased rapidly, and these structures can be found in several configurations [1] such as nanoparticles [2–4], aerogels [5], or thin films [6]. In particular, thin film nanomaterials have gained a lot of interest because they have the advantage of a simpler synthesis yielding a robust platform for design [7–9] that allows the fabrication of many nano-structures with diverse applications in optoelectronics [10], in solar cells [11], and even in portable nano-sensors using effects such as surface enhanced Raman scattering (SERS) [12]. Particularly interesting nano-systems are one-dimensional photonic crystals (1D-PhC), periodic multilayered systems that exhibit an optical band gap whose properties allow them to be used as a sensing platform [13,14], such as an electromagnetic field assisted SERS sensor [15]. Diverse electromagnetic (EM) models have been implemented to understand the optical response of the thin films, and to obtain information from complex nanostructures embedded within the structure taking advantage of non-invasive and non-destructive techniques such

as ultraviolet–visible (UV–Vis) spectroscopy [16,17]. However, while many synthesis methods yield fluctuations of the geometric parameters of the nanostructures, the roughness of the interfaces has usually not been taken into account explicitly in the design or modeling of these nano-systems.

Roughness has been widely studied in regards to several optical phenomena [18] and at different wavelength scales. For one or two slab problems with up to three interfaces numerical methods have been used to solve Maxwell equations [19] and asymptotic models for coherent scattering have been applied [20]. These have been used in geophysical problems such as the study of reflections from geological layers of ground penetration radar signals. Nevertheless, these EM models are difficult to apply in multilayered problems. Roughness has also been considered in numerical simulations using finite differences in the time domain (FDTD) for 1D-PhC in the microwave region, and it has been shown to produce appreciable red shifts of high frequency features [21], a prediction that has been experimentally confirmed. There have been some efforts to model the coherent scattering for multilayered systems with rough interfaces in the microwave region employing the Kirchhoff approximation (KA) [22]. Infinite 1D-PhC's composed of non-dispersive, non-dissipative media with rough interfaces have also been analyzed via 2D FDTD simulations [23]. For the case of wavelengths much larger than the period and for roughness heights not

exceeding some small fraction of the period, their reflectance could be reproduced as well using an homogenization procedure [24]. Unfortunately these approaches do not take into account energy losses through scattering. Diffuse light scattering for surfaces with 1D roughness has also been studied [25]. There is a lot of work done on roughness effects on wave propagation [18,26,27], but many of these EM models are not easily carried to the case of 1D-PhC. Recently, a matrix formulation of the effects of roughness [28] has been developed for multilayered structures, but it cannot be easily incorporated into the convenient and well known transfer matrix method (TMM) [29] since it doesn't yield unimodular matrices. In this work we present a TMM for stratified systems, such as 1D-PhC, that incorporates the roughness of the interfaces under the assumption of a small angle condition [30]. Under this condition, the scattering matrices [27] may be appropriately averaged to yield *macroscopic* interfacial transfer matrices that can be combined with those of other films and interfaces to produce the full transfer matrix of the system, from which all of its optical properties can be obtained readily. These transfer matrices are consistent with the well known [26, 31] Kirchhoff approximation (KA), whose validity has been widely discussed [20,22,32,33].

To test our formalism, we apply it to several systems and we compare its predictions to some experimental results. We first analyze the measured reflectance of a single nanoporous anodic alumina (NAA) film. We have selected NAA thin films due to their reproducibility [34] and versatile control through chemical means [35] for diverse applications [36]. By applying periodic current or voltage pulses during the anodizing process, NAA 1D-PhC may be obtained [13,37]. Thus, we also study with our formalism their photonic band structure, their reflectance and transmittance, and we compare the effects of constant roughness to those of progressive roughness, dissipation, and thickness fluctuations. As NAA 1D-PhC structures have been reported to yield the best detection limits as sensor devices [35,36], for quantifying optically the presence of analytes [38], we also analyze within our theory experimental NAA 1D-PhC data, expecting that incorporation of roughness considerations may lead to better sensor designs.

The structure of the paper is the following, in Sec. 2 we present our theory and we derive expressions for the transfer matrices of rough interfaces whose profile is uncorrelated to those of their neighbors interfaces, and we show how they can be incorporated into the usual transfer matrix of a multilayered system. In Appendix A we extend this theory to account for the possibility of several mutually correlated interfaces. In Sec. 3 we apply our formalism to study the reflectance of a single rough slab and we make a detailed comparison between the sample parameters obtained directly from SEM and AFM images to those fitted from the optical reflectance using our model. In Appendix B we provide details of the preparation and characterization of our samples and of our optical measurements. In Sec. 4 we study infinite and finite 1D-PhC's, obtain their band structure and relate them to their reflectance. We compare the effects of roughness to those of absorption and of thickness' fluctuations. We use these results in Sec. 5 where we measure and model the reflectance spectrum of a finite NAA 1D-PhC. Finally, Sec. 6 is devoted to our conclusion.

2. Theory

In this section we develop first the usual theory of transfer matrices for our stratified media with nominal flat interfaces in order to establish our notation. Then, we will show how to incorporate the roughness of the actual interfaces into the transfer matrix formalism under some simplifying assumptions.

2.1. Flat interfaces

We assume that the nominal system is time invariant and has translational symmetry along the xy plane, so that we can consider fields with a well defined frequency ω and 2D wavevector $\boldsymbol{Q}$ along xy, and we write the electric and magnetic fields as $\boldsymbol{E}(\boldsymbol{r},t) = \text{Re } \boldsymbol{E}(z)\exp(i\boldsymbol{Q}\cdot\boldsymbol{r}_\parallel - \omega t)$ and $\boldsymbol{H}(\boldsymbol{r},t) = \text{Re } \boldsymbol{H}(z)\exp(i\boldsymbol{Q}\cdot\boldsymbol{r}_\parallel - \omega t)$, where $\boldsymbol{r}_\parallel$ is the projection of the position vector onto the xy plane, and $\boldsymbol{E}(z)$ and $\boldsymbol{H}(z)$ are complex amplitudes at each height z. We define $\boldsymbol{E}_\parallel(z)$ and $\boldsymbol{H}_\parallel(z)$ as the projections of $\boldsymbol{E}(z)$ and $\boldsymbol{H}(z)$ onto the xy plane. For local isotropic media and given Q, the directions of $\boldsymbol{E}_\parallel(z)$ and $\boldsymbol{H}_\parallel(z)$ are well defined for both TE and TM polarizations, so we can represent them by their scalar components $E_\parallel(z)$ and $H_\parallel(z)$. The transfer matrix $\mathbf{M}(z_2,z_1)$ is a 2×2 matrix that relates $E_\parallel$ and $H_\parallel$ evaluated at two arbitrary heights z_1 and z_2,

$$\begin{pmatrix} E_\parallel \\ H_\parallel \end{pmatrix}_{z_2} = \mathbf{M}(z_2,z_1)\begin{pmatrix} E_\parallel \\ H_\parallel \end{pmatrix}_{z_1}. \tag{1}$$

Several equivalent formulations have been proposed to obtain $\mathbf{M}$ [39–41]. Within a homogeneous nonmagnetic layer α characterized by a dielectric function ε_α and refractive index $n_\alpha = \sqrt{\varepsilon_\alpha}$, the field is in general the sum of upward ($+$) and downward ($-$) going *plane* waves, with wavevector components $k_\alpha^\pm = \pm k_\alpha$ along z given by the dispersion relation

$$Q^2 + k_\alpha^2 = \varepsilon_\alpha\frac{\omega^2}{c^2}. \tag{2}$$

For economy in notation, we will use the nomenclature of plane waves even if Q is large, or ε is negative or complex, in which case, k_α may acquire an imaginary part and the waves become evanescent. We define k_α as the solution of (2) with a positive imaginary part. The surface impedance is defined as the quotient

$$Z = E_\parallel/H_\parallel. \tag{3}$$

From Faraday's and Ampere-Maxwell's equations we obtain

$$Z_\alpha^\pm = \pm Z_\alpha = \pm \begin{cases} \dfrac{\omega}{k_\alpha c}, & \text{(TE)} \\[2mm] \dfrac{k_\alpha c}{\omega\varepsilon_\alpha}, & \text{(TM)} \end{cases} \tag{4}$$

for upwards ($+$) and downwards ($-$) moving plane waves. It is convenient to write $E_\parallel(z)$ and $H_\parallel(z)$ in terms of the electric field amplitude of the $\pm$ waves for TE polarization and in terms of the magnetic field amplitudes for TM polarization. Denoting these amplitudes as $\gamma^\pm(z)$ in both cases, we write

$$\begin{pmatrix} E_\parallel \\ H_\parallel \end{pmatrix}_z = \mathbf{Q}_\alpha\begin{pmatrix} \gamma^+ \\ \gamma^- \end{pmatrix}_z, \tag{5}$$

where

$$\mathbf{Q}_\alpha = \begin{pmatrix} 1 & 1 \\ Y_\alpha & -Y_\alpha \end{pmatrix}, \quad \text{(TE)} \tag{6}$$

and

$$\mathbf{Q}_\alpha = \begin{pmatrix} Z_\alpha & -Z_\alpha \\ 1 & 1 \end{pmatrix}. \quad \text{(TM)} \tag{7}$$

Here, $Y_\alpha \equiv 1/Z_\alpha$ is the surface admittance. As $\gamma^\pm(z)$ propagate as plane waves for both polarizations, $\gamma^\pm(z) \propto \exp(\pm ik_\alpha z)$ and

$$\begin{pmatrix} \gamma^+ \\ \gamma^- \end{pmatrix}_{z_b} = \boldsymbol{P}_\alpha(z_b - z_a)\begin{pmatrix} \gamma^+ \\ \gamma^- \end{pmatrix}_{z_a} \tag{8}$$

for any z_a and z_b within the homogeneous layer, where we introduced the diagonal propagation matrix

$$\mathbf{P}_\alpha(d) = \begin{pmatrix} \exp(ik_\alpha d) & 0 \\ 0 & \exp(-ik_\alpha d) \end{pmatrix}. \tag{9}$$

Evaluating (5) at both nominal edges $z_{\alpha-1}^{(0)}$ and $z_\alpha^{(0)} = z_{\alpha-1}^{(0)} + d_\alpha$ of the layer α of width d_α and using (8) we obtain

$$\begin{pmatrix} E_{\parallel} \\ H_{\parallel} \end{pmatrix}_{z_\alpha^{(0)}} = \mathbf{M}_\alpha^{(0)} \begin{pmatrix} E_{\parallel} \\ H_{\parallel} \end{pmatrix}_{z_{\alpha-1}^{(0)}}, \tag{10}$$

where

$$\mathbf{M}_\alpha^{(0)} = \mathbf{M}_\alpha(d_\alpha) \tag{11}$$

is the transfer matrix of a homogeneous layer α that transfers the fields across its nominal width d_α,

$$\mathbf{M}_\alpha(d) = \mathbf{Q}_\alpha \mathbf{P}_\alpha(d) \mathbf{Q}_\alpha^{-1} = \begin{pmatrix} \cos(k_\alpha d) & iZ_\alpha \sin(k_\alpha d) \\ iY_\alpha \sin(k_\alpha d) & \cos(k_\alpha d) \end{pmatrix} \tag{12}$$

transfers them across a region of arbitrary width d within the homogeneous layer, and the superscript (0) in Eqs. (10) and (11) denotes absence of roughness. Notice that this transfer matrix has the same form for both TE and TM polarizations, but its value does depend on the polarization, as it is written in terms of the surface impedance and admittance of each layer, and these are polarization dependent. We remark that the determinant of this matrix is 1, as can be seen from its construction and from its components in Eq. (12), irrespective of the presence or not of dissipation, as required to comply with time reversal symmetry.

The continuity of $E_{\parallel}$ and $H_{\parallel}$ imply that the fields may be transferred from the ambient $\alpha = 0$ towards the substrate $\alpha = N+1$ through the layers $\alpha = 1...N$ by the matrix

$$\mathbf{M}^{(0)} = \mathbf{M}_N^0 \mathbf{M}_{N-1}^0 ... \mathbf{M}_2^0 \mathbf{M}_1^0. \quad \text{(nominal)} \tag{13}$$

2.2. Rough interfaces

We consider a system as above, but in which a single interface α separating medium α from $\alpha+1$ is displaced from its nominal position at $z_\alpha^{(0)}$ to a new position $z_\alpha = z_\alpha^{(0)} + \zeta_\alpha$. The transfer matrix of the modified system can then be obtained by replacing $\mathbf{M}_\alpha^{(0)}$ and $\mathbf{M}_{\alpha+1}^{(0)}$ in (13) by $\mathbf{M}_\alpha(d_\alpha + \zeta_\alpha) = \mathbf{M}_\alpha(\zeta_\alpha) \mathbf{M}_\alpha^{(0)}$ and $\mathbf{M}_{\alpha+1}(d_{\alpha+1} - \zeta_\alpha) = \mathbf{M}_{\alpha+1}^{(0)} \mathbf{M}_{\alpha+1}(-\zeta_\alpha)$ respectively. This is equivalent to the replacement of the product $\mathbf{M}_{\alpha+1}^{(0)} \mathbf{M}_\alpha^{(0)}$ by $\mathbf{M}_{\alpha+1}^{(0)} \mathbf{M}_\alpha^I \mathbf{M}_\alpha^{(0)}$, where we introduced an effective interface transfer matrix

$$\mathbf{M}_\alpha^I = \mathbf{M}_{\alpha+1}(-\zeta_\alpha) \mathbf{M}_\alpha(\zeta_\alpha). \tag{14}$$

Assuming now that all interfaces $\alpha = 0...N$ are shifted by a corresponding displacement ζ_α, we can build the complete transfer matrix as the product

$$\mathbf{M} = \mathbf{M}_N^I \mathbf{M}_N^{(0)} \mathbf{M}_{N-1}^I \mathbf{M}_{N-1}^{(0)} \mathbf{M}_{N-2}^{(0)} ... \mathbf{M}_2^I \mathbf{M}_2^{(0)} \mathbf{M}_1^I \mathbf{M}_1^{(0)} \mathbf{M}_0^I. \quad \text{(displaced)} \tag{15}$$

Now we introduce the roughness through x and y dependent height profiles $\zeta_\alpha(x,y), \alpha = 0...N$, as illustrated in Fig. 1. In the spirit of the well known Kirchhoff approximation [26,31] in the limit of low angle roughness [42], it seems tempting to apply (15) for each x, y and average it over the xy plane, or, for a randomly rough system, over all re-
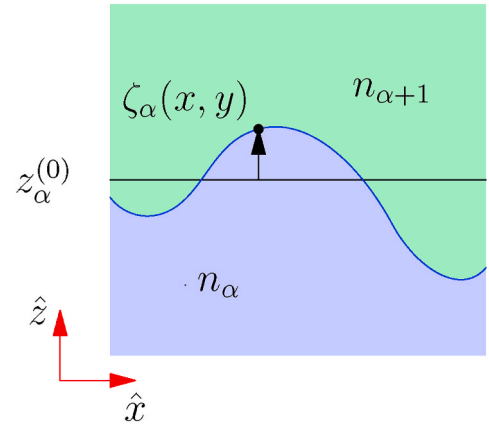

Fig. 1. Rough surface separating two consecutive layers, α and $\alpha+1$, described by refractive indices n_α and $n_{\alpha+1}$. The interface is defined through a height function $\zeta_\alpha(x,y) = z_\alpha(x,y) - z_\alpha^{(0)}$ given by its position with respect to the nominal surface $z = z_\alpha^{(0)}$.

transfer matrix *ought to be unimodular* in order to be consistent with time inversion symmetry; even though $\det \mathbf{M}_\alpha^I = \det \mathbf{M}_{\alpha+1}(-\zeta_\alpha) \det \mathbf{M}_\alpha(\zeta_\alpha) = 1$, $\det \langle \mathbf{M}_\alpha^I \rangle = \det \langle \mathbf{M}_{\alpha+1}(-\zeta_\alpha) \mathbf{M}_\alpha(\zeta_\alpha) \rangle \neq 1$. Nevertheless, the scattering matrix of each interface *is* a quantity that may be safely and meaningfully averaged.

We define the scattering $\mathbf{S}_\alpha$ matrix for the α-th interface as

$$\mathbf{S}_\alpha = \begin{pmatrix} r_\alpha^+ & t_\alpha^- \\ t_\alpha^+ & r_\alpha^- \end{pmatrix}, \tag{16}$$

as it produces the outgoing waves $\gamma_\alpha^-(z) = O_\alpha^- \exp(-ik_\alpha(z - z_\alpha^{(0)}))$ and $\gamma_{\alpha+1}^+(z) = O_\alpha^+ \exp(ik_{\alpha+1}(z - z_\alpha^{(0)}))$ when applied to the incoming waves $\gamma_\alpha^+(z) = I_\alpha^+ \exp(ik_\alpha(z - z_\alpha^{(0)}))$ and $\gamma_{\alpha+1}^-(z) = I_\alpha^- \exp(-ik_{\alpha+1}(z - z_\alpha^{(0)}))$, namely,

$$\begin{pmatrix} O_\alpha^- \\ O_\alpha^+ \end{pmatrix} = \mathbf{S}_\alpha \begin{pmatrix} I_\alpha^+ \\ I_\alpha^- \end{pmatrix}, \tag{17}$$

where we defined the amplitudes $O_\alpha^\pm$ and $I_\alpha^\pm$ using the nominal plane $z = z_\alpha^{(0)}$ as a reference, and where $r_\alpha^\pm$ and $t_\alpha^\pm$ are the reflection and transmission amplitudes corresponding to waves that impinge on the interface α moving upwards (+) within layer α or moving downwards (−) within layer $\alpha+1$. We may characterize the fields above and below the interface in terms of the components of $\mathbf{S}_\alpha$. For definitiveness, consider the case of TE polarization. For z within layer $\alpha+1$ we may write the electric and magnetic fields as $E_{\parallel}(z) = \gamma_{\alpha+1}^+(z) + \gamma_{\alpha+1}^-(z) = O_\alpha^+ \exp(ik_{\alpha+1}(z - z_\alpha^{(0)}))$ $+ I_\alpha^- \exp(-ik_{\alpha+1}(z - z_\alpha^{(0)}))$ and $H_{\parallel}(z) = Y_{\alpha+1}(\gamma_{\alpha+1}^+(z) - \gamma_{\alpha+1}^-(z)) = Y_{\alpha+1}(O_\alpha^+ \exp(ik_{\alpha+1}(z - z_\alpha^{(0)})) - I_\alpha^- \exp(-ik_{\alpha+1}(z - z_\alpha^{(0)})))$. Substituting

$$\begin{pmatrix} E_{\parallel} \\ H_{\parallel} \end{pmatrix}_z = \begin{pmatrix} t_\alpha^+ \exp(ik_{\alpha+1}(z - z_\alpha^{(0)})) & (1 + r_\alpha^-) \exp(-ik_{\alpha+1}(z - z_\alpha^{(0)})) \\ Y_{\alpha+1} t_\alpha^+ \exp(ik_{\alpha+1}(z - z_\alpha^{(0)})) & -Y_{\alpha+1}(1 - r_\alpha^-) \exp(-ik_{\alpha+1}(z - z_\alpha^{(0)})) \end{pmatrix} \begin{pmatrix} I_\alpha^+ \\ I_\alpha^- \end{pmatrix} \quad \text{(TE)} \tag{18}$$

alizations of an ensemble. For the case of mutually uncorrelated profiles, this would be equivalent to a replacement of $\mathbf{M}_\alpha^I$ by its average $\langle \mathbf{M}_\alpha^I \rangle$. Nevertheless, this would be *wrong*; the transfer matrix *is not* a quantity that may be meaningfully averaged, as the determinant of the average doesn't agree in general with the average of the determinant, and the

O_α^+ from Eq. (17), we write

and extrapolate to the nominal surface

$$\begin{pmatrix} E_\parallel \\ H_\parallel \end{pmatrix}_{z_\alpha^{(0+)}} = \mathbf{A}_\alpha \begin{pmatrix} I_\alpha^+ \\ I_\alpha^- \end{pmatrix} \quad \text{(TE)} \tag{19}$$

where

$$\mathbf{A}_\alpha = \begin{pmatrix} t_\alpha^+ & 1 + r_\alpha^- \\ Y_{\alpha+1} t_\alpha^+ & -Y_{\alpha+1}(1 - r_\alpha^-) \end{pmatrix}. \quad \text{(TE)} \tag{20}$$

In Eq. (19) we denote by $z_\alpha^{(0+)}$ the extrapolation $z \to z_\alpha^{(0)}$ towards the nominal surface within the layer $\alpha + 1$, regardless of the relative height z_α of its actual boundary with respect to that of the nominal surface. Similarly, denoting by $z_\alpha^{(0-)}$ the extrapolation towards $z_\alpha^{(0)}$ within the layer α, we write

$$\begin{pmatrix} E_\parallel \\ H_\parallel \end{pmatrix}_{z_\alpha^{(0-)}} = \mathbf{B}_\alpha \begin{pmatrix} I_\alpha^+ \\ I_\alpha^- \end{pmatrix} \quad \text{(TE)} \tag{21}$$

where

$$\mathbf{B}_\alpha = \begin{pmatrix} 1 + r_\alpha^+ & t_\alpha^- \\ Y_\alpha(1 - r_\alpha^+) & -Y_\alpha t_\alpha^- \end{pmatrix}. \quad \text{(TE)} \tag{22}$$

Similar calculations for TM polarization yield anew Eqs. (19) and (21), but with

$$\mathbf{A}_\alpha = \begin{pmatrix} Z_{\alpha+1} t_\alpha^+ & -Z_{\alpha+1}(1 - r_\alpha^-) \\ t_\alpha^+ & 1 + r_\alpha^- \end{pmatrix} \quad \text{(TM)} \tag{23}$$

and

$$\mathbf{B}_\alpha = \begin{pmatrix} Z_\alpha(1 - r_\alpha^+) & -Z_\alpha t_\alpha^- \\ 1 + r_\alpha^+ & t_\alpha^- \end{pmatrix}. \quad \text{(TM)} \tag{24}$$

As $E_\parallel(z_\alpha^{(0+)})$ and $H_\parallel(z_\alpha^{(0+)})$ are related to $E_\parallel(z_\alpha^{(0-)})$ and $H_\parallel(z_\alpha^{(0-)})$ through the interface transfer matrix, we may relate $\mathbf{A}_\alpha$ and $\mathbf{B}_\alpha$ to $\mathbf{M}_\alpha^I$ and write

$$\mathbf{M}_\alpha^I = \mathbf{A}_\alpha \mathbf{B}_\alpha^{-1}. \tag{25}$$

For a flat displaced interface we can obtain the elements of the scattering matrix either from Eqs. (14) and (25) or through a simple extrapolation of the fields from the actual towards the nominal interface,

$$\mathbf{S}_\alpha = \begin{pmatrix} r_\alpha^{(0)+}\exp(2ik_\alpha\zeta_\alpha) & t_\alpha^{(0)-}\exp(-i\Delta k_\alpha\zeta_\alpha) \\ t_\alpha^{(0)+}\exp(-i\Delta k_\alpha\zeta_\alpha) & r_\alpha^{(0)-}\exp(-2ik_{\alpha+1}\zeta_\alpha) \end{pmatrix} \tag{26}$$

where $r_\alpha^{(0)\pm}$ and $t_\alpha^{(0)\pm}$ are the Fresnel coefficients of the nominal interface [43] and $\Delta k_\alpha = k_{\alpha+1} - k_\alpha$. Thus, not unexpectedly, the effect of a rigid shift of an interface is to incorporate simple *phase* factors proportional to ζ_α into the optical coefficients. The interfacial matrix (14) can be recovered in this case from Eqs. (20)-(26).

Going back to a rough interface, in the spirit of the Kirchhoff approximation for low angle surfaces [26,27], we average (26),

$$\langle \mathbf{S}_\alpha \rangle \equiv \begin{pmatrix} \langle r_\alpha^+ \rangle & \langle t_\alpha^- \rangle \\ \langle t_\alpha^+ \rangle & \langle r_\alpha^- \rangle \end{pmatrix} = \begin{pmatrix} r_\alpha^{(0)+}\langle\exp(2ik_\alpha\zeta_\alpha)\rangle & t_\alpha^{(0)-}\langle\exp(-i\Delta k_\alpha\zeta_\alpha)\rangle \\ t_\alpha^{(0)+}\langle\exp(-i\Delta k_\alpha\zeta_\alpha)\rangle & r_\alpha^{(0)-}\langle\exp(-2ik_{\alpha+1}\zeta_\alpha)\rangle \end{pmatrix}, \tag{27}$$

we replace the optical coefficients by their averages in Eqs. 20–24 to obtain $\langle \mathbf{B}_\alpha \rangle$ and $\langle \mathbf{A}_\alpha \rangle$ and transferring the averaged fields across the nominal interface we obtain, in analogy with (25), the *macroscopic* interface transfer matrix $\mathbf{M}_\alpha^{MI}$ as

$$\mathbf{M}_\alpha^{MI} = \langle \mathbf{A}_\alpha \rangle \langle \mathbf{B}_\alpha \rangle^{-1}. \tag{28}$$

Notice that, as $\mathbf{A}_\alpha$ and $\mathbf{B}_\alpha$ are not independent, the macroscopic interface matrix (28) differs from the average of the local interface matrix (25), $M_\alpha^{MI} \neq \langle \mathbf{M}_\alpha^I \rangle$.

From Eqs. (20), (22) and (27), we notice that for TE polarization

$$\det\langle \mathbf{A}_\alpha \rangle = -2Y_{\alpha+1} t_\alpha^{(0)+} \langle\exp(-i\Delta k_\alpha\zeta_\alpha)\rangle \tag{29}$$

and

$$\det\langle \mathbf{B}_\alpha \rangle = -2Y_\alpha t_\alpha^{(0)-} \langle\exp(-i\Delta k_\alpha\zeta_\alpha)\rangle. \tag{30}$$

Nevertheless, from Fresnel's formulae we obtain

$$Y_\alpha t_\alpha^{(0)-} = Y_{\alpha+1} t_\alpha^{(0)+}, \tag{31}$$

so that $\det\langle \mathbf{A}_\alpha \rangle = \det\langle \mathbf{B}_\alpha \rangle$ and from (28) we verify the required unimodularity condition

$$\det\mathbf{M}_\alpha^{MI} = 1. \tag{32}$$

It is trivially verified that this condition also holds for TM polarization.

Finally, we get a *macroscopic* unimodular transfer matrix $\mathbf{M}^M$ for the complete system by replacing all the interface transfer matrices in (15) by their macroscopic counterparts (28),

$$\mathbf{M}^M = \mathbf{M}_N^{MI}\mathbf{M}_N^{(0)}\mathbf{M}_{N-1}^{MI}\mathbf{M}_{N-1}^{(0)}\mathbf{M}_{N-2}^{MI}...\mathbf{M}_2^{MI}\mathbf{M}_2^{(0)}\mathbf{M}_1^{MI}\mathbf{M}_1^{(0)}\mathbf{M}_0^{MI}. \tag{33}$$

We remark that although our formulation is close to that of [28], their **W** matrix is not unimodular.

From the transfer matrix of the system we may obtain its optical properties straightforwardly using standard procedures. For example, the reflection and transmission amplitudes, r and t, when the system is illuminated from the ambient towards the substrate, may be obtained by solving the 2×2 system of equations

$$\begin{pmatrix} t \\ Y_{N+1} t \end{pmatrix} = \mathbf{M}^M \begin{pmatrix} 1 + r \\ Y_0(1 - r) \end{pmatrix}, \quad \text{(TE)} \tag{34}$$

and

$$\begin{pmatrix} Z_{N+1} t \\ t \end{pmatrix} = \mathbf{M}^M \begin{pmatrix} Z_0(1 - r) \\ 1 + r \end{pmatrix}. \quad \text{(TM)} \tag{35}$$

Naturally, we define the nominal positions $z_\alpha^{(0)}$ by demanding $\langle \zeta_\alpha \rangle = 0$. Thus, in the limit of small height roughness we may approximate (27) to order ζ_α^2 by

$$\langle \mathbf{S}_\alpha \rangle = \begin{pmatrix} r_\alpha^{(0)+}(1 - 2k_\alpha^2\tilde\zeta_\alpha^2) & t_\alpha^{(0)-}\left(1 - \frac{1}{2}(\Delta k_\alpha)^2\tilde\zeta_\alpha^2\right) \\ t_\alpha^{(0)+}\left(1 - \frac{1}{2}(\Delta k_\alpha)^2\tilde\zeta_\alpha^2\right) & r_\alpha^{(0)-}(1 - 2k_{\alpha+1}^2\tilde\zeta_\alpha^2) \end{pmatrix}, \tag{36}$$

where $\tilde\zeta_\alpha \equiv \langle\zeta_\alpha^2\rangle^{1/2}$ is the RMS height, so that all optical coefficients are reduced by a factor of order $\tilde\zeta_\alpha^2/\lambda^2$, with λ the free space wavelength. This wavelength-dependent reduction is due to the energy that is lost through scattering out of the specular direction and plays a role analogous but not identical to dissipation [44]. On the other hand, if ζ_α is not necessarily small but obeys a Gaussian distribution with zero mean, we may evaluate (27) to obtain

$$\langle \mathbf{S}_\alpha \rangle = \begin{pmatrix} r_\alpha^{(0)+}\exp\left(-2k_\alpha^2\tilde{\zeta}_\alpha^2\right) & t_\alpha^{(0)-}\exp\left(-(\Delta k_\alpha)^2\tilde{\zeta}_\alpha^2/2\right) \\ t_\alpha^{(0)+}\exp\left(-(\Delta k_\alpha)^2\tilde{\zeta}_\alpha^2/2\right) & r_\alpha^{(0)-}\exp\left(-2k_{\alpha+1}^2\tilde{\zeta}_\alpha^2\right) \end{pmatrix}. \tag{37}$$

A simple substitution of any of these into (28) yields the corresponding interface matrix $\mathbf{M}_\alpha^{MI}$. Thus, in the small roughness case (36) we obtain

$$\mathbf{M}_\alpha^{MI} = \begin{pmatrix} 1 + \dfrac{(Z_{\alpha+1} - Z_\alpha)(k_\alpha + k_{\alpha+1})^2}{2(Z_\alpha + Z_{\alpha+1})}\tilde{\zeta}_\alpha^2 & -\dfrac{(Z_\alpha k_\alpha - Z_{\alpha+1} k_{\alpha+1})^2}{(Z_\alpha + Z_{\alpha+1})}\tilde{\zeta}_\alpha^2 \\ -\dfrac{(Z_{\alpha+1} k_\alpha - Z_\alpha k_{\alpha+1})^2}{(Z_\alpha + Z_{\alpha+1})Z_\alpha Z_{\alpha+1}}\tilde{\zeta}_\alpha^2 1 & -\dfrac{(Z_{\alpha+1} - Z_\alpha)(k_\alpha + k_{\alpha+1})^2}{2(Z_\alpha + Z_{\alpha+1})}\tilde{\zeta}_\alpha^2 \end{pmatrix}, \tag{38}$$

and in the general case, we obtain

$$\mathbf{M}_\alpha^{MI} = \frac{\langle t_\alpha^+ \rangle}{2}\begin{pmatrix} 1 & Z_\alpha \\ Y_{\alpha+1} & Z_\alpha Y_{\alpha+1} \end{pmatrix}$$

$$+ \frac{1}{2\langle t_\alpha^- \rangle}\begin{pmatrix} \left(1 + \langle r_\alpha^- \rangle\right)\left(1 - \langle r_\alpha^+ \rangle\right) & -\left(1 + \langle r_\alpha^- \rangle\right)\left(1 + \langle r_\alpha^+ \rangle\right)Z_\alpha \\ -\left(1 - \langle r_\alpha^- \rangle\right)\left(1 - \langle r_\alpha^+ \rangle\right)Y_{\alpha+1} & \left(1 - \langle r_\alpha^- \rangle\right)\left(1 + \langle r_\alpha^+ \rangle\right)Z_\alpha Y_{\alpha+1} \end{pmatrix} \tag{39}$$

For a Gaussian roughness we can further substitute (37).

In summary, we have developed a formalism that allows us to calculate the macroscopic effective transfer matrix of a multilayered system with rough interfaces using the Kirchhoff small-angle roughness approximation. The transfer matrix is the product of the usual transfer matrices for each layer, corresponding to their nominal width, alternating with interface transfer matrices which can be obtained from the average of the corresponding scattering matrices. We obtained explicit expressions in terms of the variance of the height of the interface for the case of small-height roughness and for the case of Gaussian roughness. In the following sections, we will illustrate the use of these matrices to calculate the optical properties of some rough stratified systems and we will compare some of our results to experiment. In Appendix A we extend the above theory to account for the possibility of several mutually correlated interfaces.

3. Application I: nanoporous anodic alumina single rough film

In this section, we first test the proposed model on a single rough film of nanoporous anodic alumina (NAA) over an Al substrate. The sample preparation and the experimental procedures are described in detail in Appendix B. We measured with an atomic force microscope (AFM) the surface profile ζ, its RMS mean $\tilde{\zeta}$, the profile slope $s = |\nabla_\parallel \zeta|$ and its RMS mean $\tilde{s}$, averaging over several positions on each sample. All studied samples exhibited $\tilde{s} < 0.02$, so that the small-angle roughness approximation holds, giving us confidence in the use of the Kirchhoff approximation.

Analysis of 3 samples: S1 is an electropolished Al substrate. S2 and S3 are NAA films on Al prepared through different anodizing conditions. t denotes the anodizing time, V or J denote either the voltage (in volts) or the current density (in mA/cm^2) applied in the corresponding *electrolyte* (see Appendix B for details). $\tilde{\zeta}$ is the RMS roughness, d the thickness of the film, and P the alumina porosity. The characterization was done through AFM (indicated by *) or SEM (†). The fit was done by modeling the reflectance.

The samples were characterized using a scanning electron microscope (SEM) to measure their thickness d and porosity P and an atomic force microscope (AFM) to determine their roughness. The uncertainties are around 10–15% for parameters defined by the SEM and AFM measurements.

As an example, in Fig. 2 we show some of the analyzed images for the sample S2, including top- and side-view SEM micro-graphs and an AFM height map.

We developed a computational code in the PERL/PDL language [45] to identify and measure the pores from our SEM images and draw their porosity maps. In essence, after eliminating small scale fluctuations, the code converts the SEM image to a high contrast black and white picture from whose average the porosity may be read and from whose borders the pores may be visualized. We analyzed several images from different regions of each sample in order to estimate the error in this procedure, which turned out to be of 10%. In Fig. 2a we superposed the porosity map on the SEM top view image. We obtained the thickness from the side view (Fig. 2b) using the ImageJ package [46]. Notice that our sample has texture on two scales, as can be observed in the AFM image (Fig. 2c). The smallest one corresponds to the pores, and we deal with it by homogenizing it using an effective medium theory [47]. The remaining texture is dealt through our transfer matrix model for rough layers.

We measured the reflectance as described in Appendix B for the 3 samples described in Table 1. We fitted the results using (33) and the
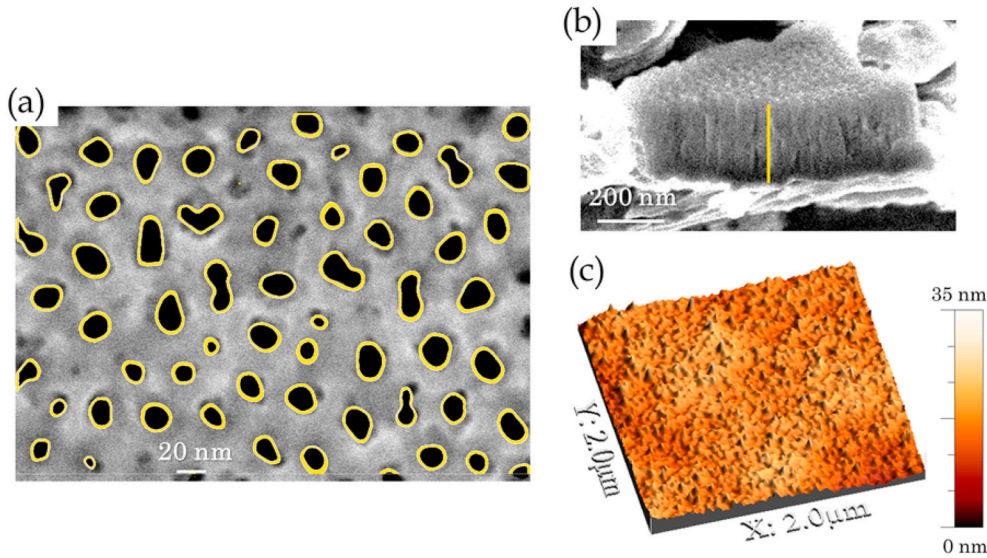

Fig. 2. Some of the images used to characterize the sample S2. (a) Top-view SEM image with a porosity map superimposed (scale bar is 20 nm). (b) Side-view SEM showing the thickness of the film (scale bar is 200 nm). (c) AFM image of the surface (the vertical color code from 0 to 35 nm is indicated). (For interpretation of the references to color in this figure legend, the reader is referred to the Web version of this article.)

Table 1

Summarizes the preparation and properties of 3 samples: an electropolished Al surface (S1), as those used as substrates for S2 and S3 which correspond to NAA films grown under different anodizing conditions.

Sample	Anodization				Characterization			Fit		
	t [s]	V	J	Electrolyte	$\tilde{\zeta}^*$ [nm]	$d^\dagger$ [nm]	$P^\dagger$ [%]	$\tilde{\zeta}$ [nm]	d [nm]	P [%]
S1	300	10		HClO$_4$	2	–	–	1.5	–	–
S2	30		11.2	H$_2$SO$_4$	5	260	15	5.8	278	20
S3	30		44.8	H$_2$SO$_4$	6	1020	30	5.1	1130	30
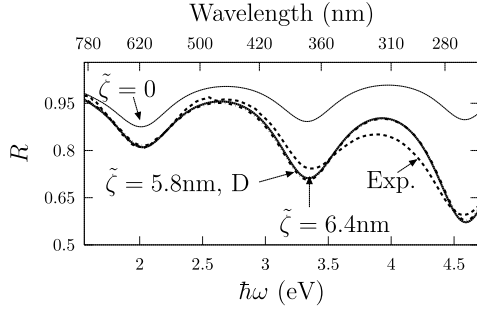
Fig. 3. Normal incidence reflectance R of sample S2 normalized to the reflectance R_0 of the substrate as a function of frequency and wavelength. We show experimental results (dashed), and several theoretical results fitted to experiment through the width d, porosity P, and/or roughness height $\tilde{\zeta}_0 = \tilde{\zeta}_1 = \tilde{\zeta}$. We show results for a flat film without dissipation ($d = 274$nm, $P = 18\%$, $\tilde{\zeta} = 0$, thin solid), a rough film without dissipation ($d = 278$, $P = 20\%$, $\tilde{\zeta} = 6.4$nm, thick solid), and a rough film with dissipation (D) due to the presence of Fe$_2$O$_3$ and CuO impurities (see text, $d = 278$nm, $P = 20\%$, $\tilde{\zeta} = 5.8$nm, dash-dotted).

Gaussian roughness model. We obtained the reflection amplitude r and the reflectance $R = |r|^2$ from Eqs. (34) and (35). As an example of our fitting procedure, in Fig. 3 we show the normal-incidence reflectance R measurement for sample S2 as a function of frequency and wavelength and the corresponding fits under different assumptions. To perform any of the calculations we need the refractive index for all the relevant media. The substrate is Al [48] while the film is NAA. The refractive index of the alumina phase was taken from Refs. [49], but to account for the nanoporous character of the film we took the porosity P as an adjustable parameter and we applied Bruggeman's 2D [47] effective media theory to obtain the index of the film. This is a very simple model but is satisfactory enough for the system under study. The fitting parameters were the RMS heights $\tilde{\zeta}_0 = \tilde{\zeta}_1 = \tilde{\zeta}$ of both interfaces (which we assumed to be equal), the thickness d and the porosity P. We obtained these three parameters using the MINUIT optimization package [50]. To that end, we developed our own computational codes using the PERL language, we used the PERL Data Language (PDL) modules for efficient numerical computation [45], and in particular, the PDL:Minuit module for interfacing to the MINUIT Fortran library developed at CERN. Fig. 3 shows that in the absence of roughness the calculated reflectance displays interference oscillations with a separation that is simply related to the nominal optical thickness of the film. Our experimental results display these oscillations, but they also show a decrease in the value of the reflectance as the frequency increases. This decay is also displayed by the fitted curve that incorporates roughness, yielding a fitted roughness of $\tilde{\zeta} = 6.4$nm. If we also account for dissipation within the alumina, due to the presence of impurities of Fe$_2$O$_3$ and CuO with concentrations 0.13% and 0.02% respectively, as corresponds to Al 1100 [51] we obtain slightly smaller fitted roughness $\tilde{\zeta} = 5.8$nm.

These results may be qualitatively understood through the wavelength dependent scattering out of the specular direction that is incorporated implicitly within our model. As discussed above (36), this effect

is of order $(\tilde{\zeta}/\lambda)^2$.

The agreement between theory and experiment for the other samples is similar to that shown in Fig. 3 for sample S2. All the fitted parameters are also included in Table 1 and for the NAA slabs correspond to the dissipative case. Notice the good agreement between the fitted parameters and the corresponding parameters obtained from AFM and SEM. For the case of the fitted parameters, the uncertainty is around 2% taking into account experimental data from different sample scanned regions.

4. One dimensional photonic crystal

We consider a 1D photonic crystal (1D PhC) consisting of the periodic alternation of two layers of refractive indices n_1 and n_2, nominal thicknesses d_1 and d_2 and period $L = d_1 + d_2$. We assume their interfaces are rough, described by small mutually uncorrelated height functions with corresponding RMS values $\tilde{\zeta}_1$ and $\tilde{\zeta}_2$. Our formulation above allows us to incorporate the effects of roughness into an effective macroscopic transfer matrix for one period by simple matrix multiplication of the appropriate interface matrices, such as

$$\mathbf{M}_L^M = \mathbf{M}_2^{MI}\mathbf{M}_2^{(0)}\mathbf{M}_1^{MI}\mathbf{M}_1^{(0)}. \tag{40}$$

The normal modes of the system are Bloch waves which are easily obtained from the transfer matrix by solving the eigenvalue problem
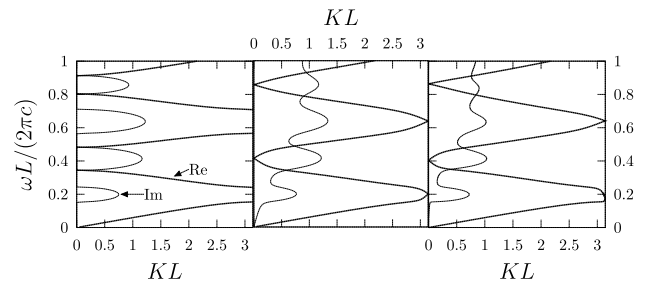
$$\mathbf{M}_L^M \begin{pmatrix} E_\parallel \\ H_\parallel \end{pmatrix}_{nL} = \Lambda \begin{pmatrix} E_\parallel \\ H_\parallel \end{pmatrix}_{nL}, \tag{41}$$

to obtain the eigenvalues

$$\Lambda_\pm = \exp(\pm iKL), \tag{42}$$

and eigenvectors

$$\begin{pmatrix} E_\parallel \\ H_\parallel \end{pmatrix}_{nL} \propto \begin{pmatrix} Z_\pm \\ 1 \end{pmatrix}, \tag{43}$$

Fig. 4. Dispersion relation of the Bloch modes propagating along the axis of an infinite 1D-PhC made of alternating layers of nominal widths $d_1 = 100$nm and $d_2 = 80$nm. We show the real (thick) and imaginary (thin) parts of the normalized Bloch wave vector KL, with L the period, as a function of the normalized frequency $\omega L/2\pi c$ for a dispersionless and dissipationless system with flat interfaces with real dielectric constants $\varepsilon_1 = 12$ and $\varepsilon_2 = 1$ (left), for the same system but with some dissipation, with $\varepsilon_1 = 12 + 1.2i$, $\varepsilon_2 = 1 + 0.1i$ (middle) and for the system without dissipation but with Gaussian rough surfaces, with $\varepsilon_1 = 12$, $\varepsilon_2 = 1$, $\tilde{\zeta}_1 = 10$nm and $\tilde{\zeta}_2 = 8$nm (right).

where K is the Bloch vector along the axis of the structure and $Z_\pm$ are the surface impedances for Bloch waves propagating (or decaying) towards $\pm z$ evaluated at the position nL, $n = 1, 2...$ corresponding to the even numbered interfaces. As the transfer matrix is unimodular, we can rewrite the dispersion relation as

$$\cos(KL) = (m_{11} + m_{22}) / 2, \tag{44}$$

where m_{ij}, $i, j = 1, 2$ are the matrix elements of $\mathbf{M}_L^M$. The impedances are

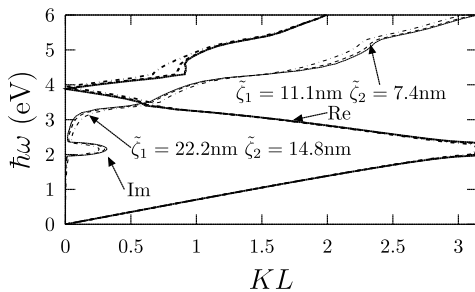$$Z_\pm = \frac{m_{12}}{\exp(\pm iKL) - m_{11}} = \frac{\exp(\pm iKL) - m_{22}}{m_{21}} \tag{45}$$

4.1. Photonic bands

In Fig. 4 we show the dispersion relation ω vs. K of the Bloch waves of an infinite 1D-PhC, calculated as discussed above for parallel wave-vector $Q = 0$.

The system consists of two alternating films with thicknesses $d_1 = 100$nm and $d_2 = 80$nm. To elucidate the role of roughness and of dissipation, we calculated the modes for three cases: dispersionless, dissipationless media with flat surfaces ($\varepsilon_1 = 12$, $\varepsilon_2 = 1$, $\tilde{\zeta}_1 = \tilde{\zeta}_2 = 0$), the same system with some dissipation artificially added ($\varepsilon_1 = 12 + 1.2i$, $\varepsilon_2 = 1 + 0.1i$, $\tilde{\zeta}_1 = \tilde{\zeta}_2 = 0$), and the same system without dissipation but with some Gaussian roughness ($\varepsilon_1 = 12$, $\varepsilon_2 = 1$, $\tilde{\zeta}_1 = 8$nm, $\tilde{\zeta}_2 = 10$nm). For the dissipative case we added an imaginary part to ε_α equal to 10% of its real part. For the rough case we chose the roughness amplitude as 10% of the width of the corresponding layer. Notice that this roughness is not small for the highest frequencies in the figure. Thus, (38) is not applicable, but we use (39). For the flat system without dissipation (Fig. 4, left) we found, as expected, bands for which the modes may propagate, with Im $K = 0$ and with alternating positive and negative group velocity, and gaps for which propagation is forbidden and the *modes* decay exponentially, with Im $K \neq 0$ and Re $K = 0$ or $\pm \pi / L$, at the center or at the edges of the Brillouin zone. The center of the gaps are at frequencies ω_m whose corresponding free-space wavelength $\lambda_m = 2\pi c/\omega_m$ is a sub-multiple of twice the optical width of a period, yielding constructive interference of the waves back-scattered by successive periods,

$$n_1 d_1 + n_2 d_2 = m\lambda_m/2, \tag{46}$$

and where Im K peaks. In the case with dissipation (Fig. 4, center), Im K also displays maxima corresponding to the gaps, but ReK for those frequencies is no longer a constant at the center or at the edges of the Brillouin zone, corresponding to both decay and propagation. There are
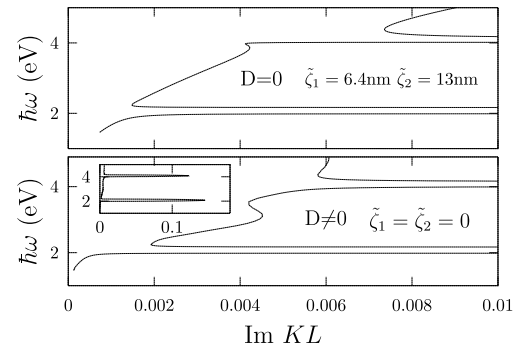
also regions where ImK becomes relatively small, corresponding to the propagating bands, but it is not zero, so there is some decay due to extinction through absorption. For high enough frequencies the minima of Im K is almost $1/L$, so that the decay distance becomes of the order of one period. Of course, these are not actual modes that may be excited within an infinite system, but they may be excited in truncated photonic crystals or in crystals with defects. In the case with roughness (Fig. 4, right), the results are very similar to those obtained in the case with dissipation, as roughness also yields extinction, though its origin is scattering out of the specular direction instead of absorption. We remark that we didn't calculate explicitly the non-specular scattered fields, but the optical theorem implies that the energy they carry away manifests itself through destructive interference in the specular term [29].

In order to explore roughness effects for realistic systems, in Fig. 5 we show the band structure for a nanoporous anodic silicon (NAS) 1D-PhC made of two alternating layers with porosities $p_1 = 73\%$ and $p_2 = 54\%$ and widths $d_1 = 111$nm and $d_2 = 74$nm, as obtained from Ref. [52]. We obtained ε_α from the porosity p_α and the dielectric function of silicon, taken from Palik's handbook [48], using the Bruggeman 2D model [47]. In Fig. 5 we show results corresponding to a flat structure and to a structure with rough surfaces considering two cases, a RMS height of 10% of the corresponding layer's width, i.e., $\tilde{\zeta}_1 = 11.1$nm and $\tilde{\zeta}_2 = 7.4$nm, and a RMS height of 20% of the layer's width ($\tilde{\zeta}_1 = 22.2$nm and $\tilde{\zeta}_2 = 14.8$nm). As expected, the middle of the first band gap at $\hbar\omega_1 = 2.24$eV complies with (46), with $m = 1$. For this system, the effects of dissipation dominate those of roughness. For the 10% case the roughness corrections are barely visible, though for the 20% they are relatively small but clearly discernible. We expect roughness to be more important for materials with a smaller dissipation, such as NAA.

In Fig. 6 we show the band diagram of an NAA 1D-PhC made up two alternating layers of widths $d_1 = 64$ nm and $d_2 = 130$ nm and porosities $p_1 = 7\%$ and $p_2 = 35\%$. We used Bruggeman's 2D model in order to calculate the dielectric functions ε_α ($\alpha = 1, 2$) of the porous layers from that of Al [48,51]. The calculation was done both for the case of flat interfaces but including dissipation within the alumina due to impurities of Fe_2O_3 and CuO, as in Sec. 3, and for that of rough interfaces characterized by $\tilde{\zeta}_1 = 6.4$ nm and $\tilde{\zeta}_2 = 13$nm (so that $\tilde{\zeta}_\alpha/d_\alpha = 0.1$) and without dissipation within the alumina. We plot the imaginary part of the Bloch vector K. Two band gaps are clearly seen in the band structure, consistent with (46), in which the imaginary part of Bloch's vector K has large peaks (see inset of Fig. 6) with or without roughness of the order of $0.1/L$, corresponding to small penetration depths of $\approx 10L$. Besides the gaps, there are propagation bands for which Im K would be null in the

Fig. 5. Band diagrams of Bloch modes propagating along the axis of a 1D-PhC made of nanoporous anodic silicon (NAS) layers of width $d_1 = 111$ nm with 73% porosity alternating with NAS layers of width $d_2 = 74$ nm with 54% porosity. We show the real part (thick) and imaginary part (thin) of the normalized Bloch's vector KL as a function of photon energy $\hbar\omega$. We show results for flat interfaces (solid), for rough interfaces with RMS heights $\tilde{\zeta}_1 = 11.1$nm and $\tilde{\zeta}_2 = 7.4$nm (dashed), and for rough interfaces with $\tilde{\zeta}_1 = 22.2$nm and $\tilde{\zeta}_2 = 14.8$nm (dot dashed).

Fig. 6. Band structure for a 1D-PhC of two alternating layers of NAA with porosities $p_1 = 7\%$ and $p_2 = 35\%$, and widths $d_1 = 64$ nm and $d_2 = 130$ nm. We show the normalized imaginary part of the Bloch vector Im KL as a function of energy $\hbar\omega$. We present results corresponding to a dissipationless system with rough interfaces ($D = 0$, $\tilde{\zeta}_1 = 6.4$ nm, $\tilde{\zeta}_2 = 13$nm, top), and for a system with dissipation corresponding to Fe_2O_3 and CuO impurities, as in Sec. 3, but with flat interfaces ($D \neq 0$, $\tilde{\zeta}_1 = \tilde{\zeta}_2 = 0$, bottom). The inset corresponds to a change of scale.
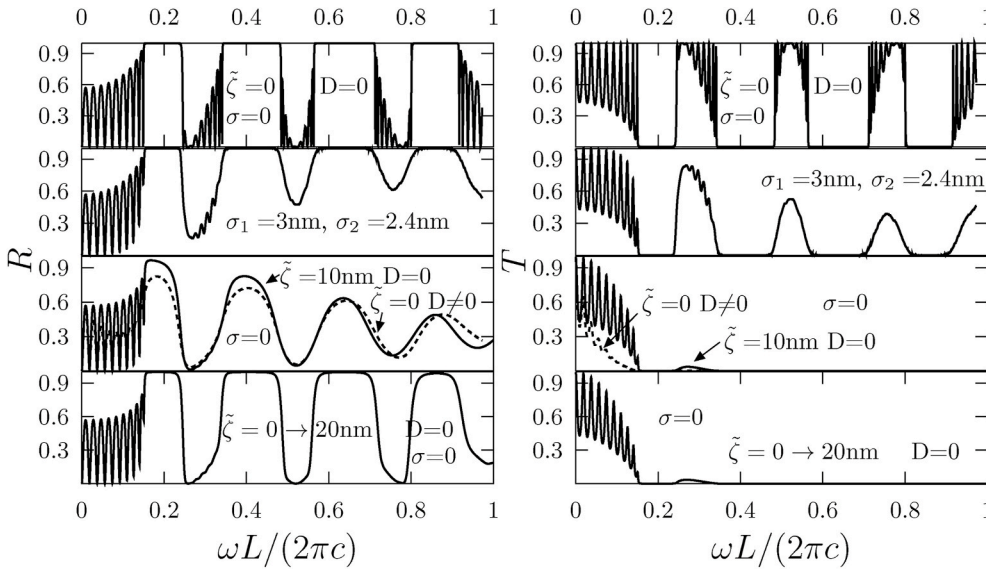
Fig. 7. Normal incidence reflectance R (left) and transmittance T (right) of a free-standing ($n_0 = n_s = 1$) finite 1D-PhC made up of $N = 10$ pairs of films of widths $d_1 = 100$nm and $d_2 = 80$nm as a function of the normalized frequency $\omega L/2\pi c$ where $L = d_1 + d_2$. We consider several cases: no dissipation ($D = 0$) corresponding to the real dielectric functions $\varepsilon_1 = 12$ and $\varepsilon_2 = 1$, with no roughness $\tilde{\zeta}_1 = \tilde{\zeta}_2 = 0$ and no fluctuations $\sigma_1 = \sigma_2 = 0$ (top row); no dissipation, no roughness and width fluctuations $\sigma_1 = 3$nm, $\sigma_2 = 2.4$nm (second row); roughness without dissipation nor fluctuations, $\tilde{\zeta}_1 = \tilde{\zeta}_2 = 10$nm, $D = 0$ and $\sigma_1 = \sigma_2 = 0$ (solid) and dissipation with no roughness nor fluctuations, $\varepsilon_1 = 12 + 1.2i$, $\varepsilon_2 = 1 + 0.1i$, $\tilde{\zeta}_1 = \tilde{\zeta}_2 = 0$ and $\sigma_1 = \sigma_2 = 0$ (dashed) (third row); roughness growing linearly with height $\zeta_1 = \zeta_2 = 0 \rightarrow 20$nm without dissipation nor fluctuations (bottom row).

absence of roughness and dissipation. Nevertheless, $\text{Im}K \neq 0$ for the rough system and takes values as high as $K \approx 0.005/L$ corresponding to a penetration distance of at most ≈ 200 periods. For the parameters chosen, the effects of roughness are qualitatively similar to those of dissipation.

4.2. Finite 1D-PhC

Now, we consider a finite stratified system of width NL made from N repetitions of a unit cell composed of two layers of nominal thicknesses d_1 and $d_2 = L - d_1$, refractive indices n_1 and n_2, and with mutually uncorrelated rough surfaces characterized by the RMS heights $\tilde{\zeta}_1$ and $\tilde{\zeta}_2$, respectively. The refractive index of ambient is n_0 while for the substrate is $n_{2N+1} = n_s$. We can obtain the reflectance and transmittance of the system from Eqs. 33–35.

In Fig. 7 we show the normal incidence reflectance R and transmittance T spectra of a free standing finite 1D-PhC in air ($n_0 = n_s = 1$) consisting of $N = 10$ periods of the same photonic crystals as in Fig. 4, with and without dissipation and roughness. We also present results for a system with flat surfaces and no roughness nor dissipation, but whose thicknesses have mutually uncorrelated fluctuations, and for a system without dissipation nor width fluctuations but with a roughness whose amplitudes grow linearly from the surface towards the substrate. As shown in the top row of Fig. 7, in the case without dissipation, roughness nor fluctuations, there are relatively wide regions of very high reflectance $R \approx 1$ and very small transmittance $T \approx 0$ corresponding to the band gaps shown in Fig. 4. Outside of these regions, the reflectance and transmittance show strong oscillations due to the interference of the waves reflected from the front and back surfaces of the system. These oscillations take R to values as low as 0. Correspondingly, T takes values as high as 1.

In the second row of Fig. 7, we show the reflectance and transmittance averaged over an ensemble of 1D-PhC's as those corresponding to the first row, but with fluctuations in the widths of each film obeying a Gaussian distribution with standard deviations $\sigma_1 = 3$nm and $\sigma_2 = 2.4$nm corresponding to 3% of their nominal widths. We used one thousand ensemble members for our calculation. The purpose of this calculation is to allow for a finite transverse coherence length ξ [29] for the incident light, so that the contributions to the reflectance and transmittance from illuminated regions farther apart than ξ add incoherently. This situation will prove relevant for the system studied in the next section.

The results show regions where $R \approx 1$ and $T \approx 0$ as in the top row,

but the oscillating structure due to the interference is damped by the averaging process, as the frequencies corresponding to each maxima and minima differ for each member of the ensemble. This damping is larger at higher frequencies, for which the oscillations displayed by the first row become narrower and their frequency spacing becomes smaller. The third row of Fig. 7 shows the effects of roughness characterized by the amplitudes $\tilde{\zeta}_1 = \tilde{\zeta}_2 = 10$nm. In this case, R shows maxima corresponding to the band gaps of Fig. 4, but they don't attain the value 1, as in the top and second rows. The reason is that in this case, energy is lost through scattering, reducing the specular reflectance. In our treatment of roughness, we averaged scattering matrices, thus incorporating phase information that is not present in our treatment of thickness fluctuations corresponding to the second row of Fig. 7, for which we averaged the reflectance and transmittance. Hence the qualitative differences. Corresponding to the maxima in R for the case of a rough surface there are minima in T. Nevertheless, most of the energy is reflected or scattered away so that beyond $\omega \approx 0.3 \times 2\pi c/L$ the transmittance becomes negligible. The third row of Fig. 7 also shows results for a flat absorptive system with $\varepsilon_1 = 12 + 1.2i$ and $\varepsilon_2 = 1 + 0.1i$. The result of dissipation is similar to that of roughness without dissipation.
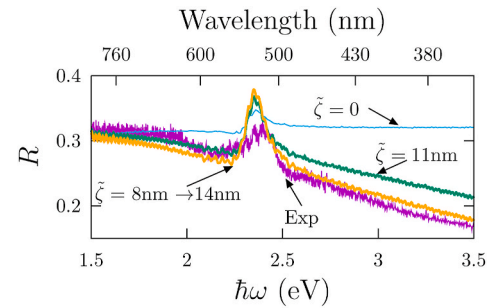
Fig. 8. Normal incidence reflectance R as a function of photon energy and wavelength for a 1D-PhC made of 60 repetitions of two alternating film of NAA. We show experimental (Exp.) and several fitted theoretical results. We show results for a system with flat surfaces ($\tilde{\zeta} = 0$), for a rough system with a height that increases linearly with depth from $\tilde{\zeta} = 8$nm up to 14 nm, and for a rough system with constant height $\tilde{\zeta} = 11$nm. We averaged R over a thousand members of an ensemble with fluctuating layer widths characterized by Gaussian distributions with standard deviations $\sigma_1 = \sigma_2 = 8$nm. In all cases we used the fitted porosities $P_1 = 29\%$ and $P_2 = 16\%$, and widths $d_1 = 90$nm and $d_2 = 87$nm.

In the bottom row of Fig. 7 we show the effect of a roughness that increases linearly in height from the front ($\tilde{\zeta} = 0$) towards the back ($\tilde{\zeta} = 20nm$) so that its average coincides with that considered in the third row. In this case, the reflectance does attain the value 1 corresponding to the band gaps, as in the first row, since within the gaps most of the electromagnetic energy is reflected before reaching the deep layers and thus it doesn't sense the larger roughness. Nevertheless, the interference oscillations of the first row corresponding to the propagating bands are smoothed out as in the second and third rows. On the other hand, the transmittance is very similar to that of the third row for all frequencies as the transmitted energy is scattered away by the rough deep layers. If we invert the roughness progression, the results would be similar to those in the third row.

In the next section we will explore a real stratified system for which the analysis of roughness that increases with depth plays a relevant role.

5. Application II: NAA 1D-PhC

We prepared an NAA 1D-PhC made of 60 repetitions of two alternating NAA layers of different porosities and widths on an Al substrate by following the procedure described in Appendix B. We used Bruggeman's 2D model [47] to calculate the dielectric response of the porous alumina layers in terms of their porosity and the alumina response. We designed the system so as to have a resonance (46) at the mid UV–Vis range.

In Fig. 8 we show the normal incidence reflectance spectrum obtained experimentally together with several fitted theoretical curves. We considered models with flat interfaces, with constant roughness and with linearly increasing roughness, incorporating in all cases thickness fluctuations.

All of the fitted spectra reproduce the reflectance maximum around 2.4eV. In the absence of roughness the curve flattens out for higher energies. Roughness yields a decrease of R for frequencies above the peak due to the extinction of the specular fields as a consequence of scattering, but the high frequency fit is much better for the case of progressive roughness. Such parameter optimization was performed using the MINUIT package. The fitted parameters are the porosities ($P_1 = 29\%$, $P_2 = 16\%$), the nominal thicknesses ($d_1 = 90nm$, $d_2 = 87nm$), the Gaussian fluctuations of the layer widths ($\sigma_1 = \sigma_2 = 8nm$), and the roughness height ($\tilde{\zeta}_1 = \tilde{\zeta}_2 = \tilde{\zeta} = 11nm$ for a constant roughness and $\zeta = 8nm - 14nm$ for linearly increasing progressive roughness). Since the current densities used for the 1D-PhC are those of S2 and S3, the fitted porosities P_2 and P_1 are similar to those reported in Table 1 and the fitted thicknesses d_i were in accordance to the expected ones, given the growth conditions used. The roughness heights are higher than for the single slabs of Sec. 3 which suggests that there exists an accumulation effect on the roughness when the unit cell is repeated several times.

6. Conclusions

We have developed a transfer matrix formalism for stratified systems such as 1D photonic crystals that is capable of incorporating in a very simple way some effects of the interface roughness. We assumed the rough surface obeys the small angle condition. Under this approximation [30] the scattering matrix [27] $\mathbf{S}_\alpha$ of each interface acquires a local phase that may be averaged to produce macroscopic interfacial transfer matrices (28) whose determinant is 1, and that may be incorporated into the transfer matrix of the whole system. The interfacial matrices are consistent with the well known [26,31] Kirchhoff approximation (KA), whose validity has been amply discussed [20,22,32,33]. From the total macroscopic transfer matrix all optical properties follow through the usual procedures for layered systems. We extended the formalism in an appendix to the case where nearby interfaces have mutually correlated roughness.

We employed our formalism to study a single NAA film on an Al substrate. We verified that our assumptions held for our samples through AFM and SEM characterizations. We observed the characteristic oscillations due to interference between the fields reflected by both interfaces of the film. Roughness yields a decrease in the reflectance for increasing frequency due to the extinction of the specular fields through increased scattering. This decrease is observed experimentally and is absent from the results for flat films. Furthermore, we found a good agreement between the parameters of the system fitted to our measurements of the reflectance and the corresponding parameters measured directly through SEM and AFM microscopy.

We also analyzed theoretically the photonic band structure of infinite periodic multilayered systems. We found that roughness has an effect similar to that of dissipation. Both blur the distinction between propagating bands and band-gaps and produce a finite decay length within the system, as extinction can be produced by scattering as well as by absorption. When both absorption and roughness are present, their effects compete and one or the other may dominate.

We studied finite slices of photonic crystals and compared the effects of roughness to dissipation and to fluctuations in the film widths. We found that roughness, dissipation and fluctuations in the widths eliminate the oscillations due to the interference between multiple reflections from the boundaries. Furthermore, roughness and dissipation produce a similar decrease in the reflectance maxima at the band-gaps, but width fluctuations do not. We also studied progressive roughness that increases towards the substrate, and which is expected in systems such as NAA prepared by an electrochemical attack from the front towards the back.

Finally, we applied our formalism to model the reflectance of an NAA photonic crystal on an Al substrate and compared experimental and theoretical results. Experiment and the theory show a maximum due to constructive interference of fields reflected by successive periods, but there is a decrease of the reflectance for higher frequencies which is well reproduced by the model that incorporates roughness but not by the model with flat surfaces.

In summary, we developed a very simple theory which allows us to incorporate roughness into standard transfer matrix calculations of the optical properties of stratified media. We calculated properties of single films, of finite Bragg mirrors and of infinite superlattices, and compared results to experiment. Our results show that structural parameters that may be difficult to measure directly may be obtained by analyzing optical properties and using our formalism. Thus, we conclude that when applicable, our formalism is useful and convenient.

Author agreement

All authors have seen and approved the final version of the manuscript being submitted. They warrant that the article is an original work made by them and it is not currently under consideration for publication elsewhere.

CRediT authorship contribution statement

Leandro L. Missoni: Investigation, Data curation. **Guillermo P. Ortiz:** Methodology, Software, Supervision, Writing - original draft. **María Luz Martínez Ricci:** Investigation, Writing - review & editing. **Victor J. Toranzos:** Resources, Validation. **W. Luis Mochán:** Conceptualization, Methodology, Validation, Writing - review & editing.

Declaration of competing interest

The authors declare that they have no known competing financial interests or personal relationships that could have appeared to influence the work reported in this paper.
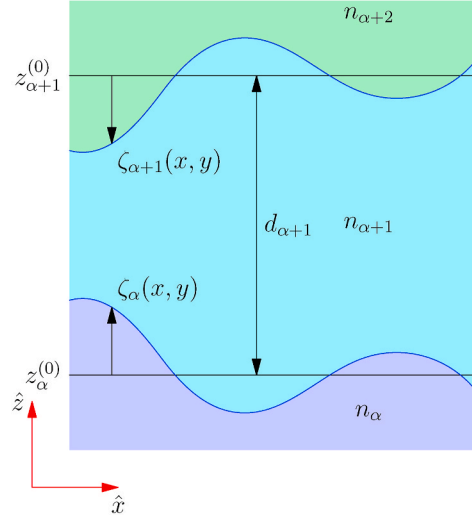
Appendix A. Correlated rough interfaces

We extend the formalism of Sec. 2 to account for correlations between two or more interfaces, as illustrated in Figure A1.

Fig. A1. Example of correlated rough interfaces. Layer $\alpha + 1$ of nominal width $d_{\alpha+1}$ and refractive index $n_{\alpha+1}$ has perfectly anti-correlated interfaces at $z_\alpha(x,y) = z_\alpha^{(0)} + \zeta_\alpha(x,y)$ and $z_{\alpha+1}(x,y) = z_{\alpha+1}^{(0)} + \zeta_{\alpha+1}(x,y)$, where $\zeta_{\alpha+1}(x,y) = -\zeta_\alpha(x,y)$.

In case the interfaces $\alpha, \alpha + 1 \ldots \alpha + n$ are correlated, we consider the corresponding contributions to the displaced transfer matrix (15)

$$\mathbf{M}_{\alpha+n,\alpha} = \mathbf{M}_{\alpha+n}^I \mathbf{M}_{\alpha+n}^{(0)} \mathbf{M}_{\alpha+n-1}^I \ldots \mathbf{M}_{\alpha+2}^I \mathbf{M}_{\alpha+1}^{(0)} \mathbf{M}_{\alpha+1}^I \mathbf{M}_\alpha^I, \tag{47}$$

we obtain its corresponding scattering matrix $\mathbf{S}_{\alpha+n,\alpha}$ relating the outgoing amplitudes O_α^- and $O_{\alpha+n}^+$ to the incoming amplitudes I_α^+ and $I_{\alpha+n}^-$ by solving Eqs. analogous to Eqs. (34) and (35), use them to construct the left and right matrices $\mathbf{B}_{\alpha+n,\alpha}$ and $\mathbf{A}_{\alpha+n,\alpha}$, average them, and use them to construct a macroscopic slab transfer matrix

$$\mathbf{M}_{\alpha+n,\alpha}^M = \langle \mathbf{A}_{\alpha+n,\alpha} \rangle \langle \mathbf{B}_{\alpha+n,\alpha} \rangle^{-1} \tag{48}$$

which may be spliced into (33) replacing the product $\mathbf{M}_{\alpha+n}^{MI} \mathbf{M}_{\alpha+n}^{(0)} \ldots \mathbf{M}_{\alpha+1}^{(0)} \mathbf{M}_\alpha^{MI}$ to obtain the macroscopic transfer matrix

$$\mathbf{M}^M = \mathbf{M}_N^{MI} \mathbf{M}_N^{(0)} \mathbf{M}_{N-1}^{MI} \ldots \mathbf{M}_{\alpha+n+1}^{MI} \mathbf{M}_{\alpha+n+1}^0 \mathbf{M}_{\alpha+n,\alpha}^M \tag{49}$$

$$\mathbf{M}_\alpha^0 \mathbf{M}_{\alpha-1}^{MI} \ldots \mathbf{M}_1^{MI} \mathbf{M}_1^{(0)} \mathbf{M}_0^{MI},$$

of the rough correlated system.

Appendix B. Experimental Section

B.1 Materials

Square plates of 20 mm side were obtained from commercial 0.8mm thick Al 1100 [51] sheets. Sulfuric (H_2SO_4) and perchloric acid ($HClO_4$) (Sigma-Aldrich) were used without further purification. Biopack absolute ethanol and ultra-pure water were used to prepare solutions. Sintorgan pure Acetone, Biopack Sodium hidroxide (NaOH), and Cicarelli Nitric acid (HNO_3) 65% were used for cleaning.

B.2 NAA Sample preparation: Thin Films and 1D-PhCs

Prior to the anodizing process, Al foils were cleaned by sequentially immersing and draining them in acetone for 5 min, in 10%m/v sodium hydroxide solution for 1 min, and nitric acid 50%v for 1 min. Afterwords, they were thoroughly rinsed in bi-distilled water.

All samples were electroplated by setting them on a stainless steel cathode with a contacting surface larger than the sample surface and applying a potential of 10–12V while immersed in a 1:4 solution of perchloric acid and absolute ethanol. As electroplating is an exothermic reaction, it was performed in a thermal bath with ice. The best electroplated Al samples, with reflectance larger than 80% and without significant dispersion in the optical spectral range, were obtained by fixing the voltage at 10V during 5min. To prepare NAA samples we applied a registered procedure [37] with

an electrolyte composed of a solution of sulfuric acid 15%m/v and used a home-made voltage and current PC controlled sources to operate the anodizing cell [53]. We have synthesized samples of NAA films and 1D-PhC's on the Al samples. NAA thin films were prepared at different current densities J and for different times t as specified in Table 1 in the manuscript. NAA 1D-PhC's were prepared by first growing a protective thick film at 15V during 600s and then by producing two alternating NAA layers at $J_1 = 44.8$mA/cm^2 for $t_1 = 4.5$s and $J_2 = 11.2$mA/cm^2 for $t_2 = 22$s. This binary unit was repeated 60 times. Following the anodizing procedure [37] to produce for each J_i several NAA films samples and by applying a linear regression of its thickness versus anodizing times we have obtained the linear growth rates $v_1 \approx 20$nm/s and $v_2 \approx 4$nm/s.

B.3 Characterization Techniques

We used an Ocean Optics USB-4000 spectrometer to measure the intensity I_0 of our deuterium-tungsten-halogen light source (DT-MINI-2 Ocean Optics), the intensity I reflected at normal incidence from the NAA films and the reference intensity I_{ref} reflected from an Al film evaporated onto a glass substrate. We adapted a reflection probe to the spectrometer above to characterize UV–Vis–NIR optical properties. Scanning Electron Microscopy (SEM) images were obtained for single NAA films using a Zeiss Ultra 55 microscope. Front views and cross-section were performed to measure porosity and thickness respectively. The porosity was determined through image analysis with a computational code and images from different regions of each sample were studied to determine the expected error. Multi-mode 8 Atomic Force Microscopy (Nanoscope V controller, Bruker, Santa Barbara) was used in contact mode to get the NAA profiles. The cantilever spring constant was 0.32 N/m.

References

[1] Song-Yuan Ding, En-Ming You, Zhong-Qun Tian, Martin Moskovits, Electromagnetic theories of surface-enhanced Raman spectroscopy, Chem. Soc. Rev. 46 (2017) 4042–4076.

[2] T.S. Ahmadi, Z.L. Wang, T.C. Green, A. Henglein, M.A. El-Sayed, Shape-controlled synthesis of colloidal platinum nanoparticles, Science 272 (1996) 1924.

[3] V.F. Puntes, K.M. Krishnan, A.P. Alivisatos, Colloidal nanocrystal shape and size control: the case of cobalt, Science 291 (2001) 2115.

[4] G. Rodriguez-Gattorno, D. Díaz, L. Rendón, G.O. Hernández-Segura, Metallic nanoparticles from spontaneous reduction of silver(i) in dmso. interaction between nitric oxide and silver nanoparticles, J. Phys. Chem. B 106 (2002) 2482.

[5] M.L. Anderson, C.A. Morris, R.M. Stroud, C.I. Merzbacher, D.R. Rolison, Colloidal gold aerogels: preparation, properties and characterization, Langmuir 15 (1999) 674–681.

[6] M.C. Fuertes, M. Marchena, M.C. Marchi, A. Wolosiuk, G.J.A.A. Soler-Illia, Controlled deposition of silver nanoparticles in mesoporous single-or multilayer thin films: from tuned pore filling to selective spatial location of nanometric objects, Small 5 (2) (2009) 272–280.

[7] Brian Geist, William B. Spillman Jr., Richard O. Claus, Thermal cycling and the optical and electrical characterization of self-assembled multilayer nile blue a–gold thin films, Appl. Optic. 44 (30) (Oct 2005) 6357–6360.

[8] E.D. Martínez, M.G. Bellino, G.J.A.A. Soler-Illia, Patterned production of silver-mesoporous titania nanocomposite thin films using lithography-assisted metal reduction, ACS Appl. Mater. Interfaces 1 (4) (2009) 746–749.

[9] Achim Fischereder, Maria Luz Martinez-Ricci, Alejandro Wolosiuk, Wernfried Haas, Ferdinand Hofer, Gregor Trimmel, J.A.A. Soler-Illia Galo, Mesoporous ZnS thin films prepared by a nanocasting route, Chem. Mater. 24 (10) (2012) 1837–1845.

[10] Claes G. Granqvist, Transparent conductors as solar energy materials: a panoramic review, Sol. Energy Mater. Sol. Cell. 91 (2007) 1529–1598.

[11] S. Colodrero, A. Mihi, J.A. Anta, M. Oca na, H. Míguez, Experimental demonstration of the mechanism of light harvesting enhancement in photonic-crystal-based dye-sensitized solar cells, J. Phys. Chem. C 113 (2009) 1150.

[12] Alejandro Wolosiuk, Nicolas G. Tognalli, Eduardo D. Martínez, Mara Granada, M Cecilia Fuertes, Horacio Troiani, Sara A. Bilmes, Alejandro Fainstein, Galo JAA. Soler-Illia, Silver nanoparticle-mesoporous oxide nanocomposite thin films: a platform for spatially homogeneous sers-active substrates with enhanced stability, ACS Appl. Mater. Interfaces 6 (7) (2014) 5263–5272.

[13] Rajesh V. Nair, R. Vijaya, Photonic crystal sensors: an overview, Prog. Quant. Electron. 34 (3) (2010) 89–134.

[14] Tushar Kumeria, Abel Santos, Mohammad Mahbubur Rahman, Josep Ferré-Borrull, Lluís F. Marsal, Dusan Losic, Advanced structural engineering of nanoporous photonic structures: tailoring nanopore architecture to enhance sensing properties, ACS Photonics 1 (12) (2014) 1298–1306.

[15] Rodrigo Martínez Gazoni, Martín G. Bellino, M. Cecilia Fuertes, Gustavo Giménez, J. Galo, A.A. Soler-Illia, María Luz Martinez-Ricci, Designed nanoparticle–mesoporous multilayer nanocomposites as tunable plasmonic–photonic architectures for electromagnetic field enhancement, J. Mater. Chem. C 5 (2017) 3445–3455.

[16] V.M. Sánchez, E.D. Martinez, M.L. Martinez-Ricci, H. Troiani, G.J.A.A. Soler-Illia, Optical properties of au nanoparticles included in mesoporous tio^2 thin films: a dual experimental and modeling study, J. Phys. Chem. C 117 (2013) 7246–7259.

[17] Diego Onna, Ignacio Perez Ipiña, Agustina Fernández Casafuz, M. Álvaro Mayoral, Ricardo Ibarra García, Sara A. Bilmes, María Luz Martínez Ricci, Diameter distribution by deconvolution (ddd): absorption spectra as a practical tool for semiconductor nanoparticle psd determination, Nanoscale Adv 1 (2019) 3499–3505.

[18] Heinz Raether, Surface Plasmons on Smooth and Rough Surface and on Gratings, Springer-Verlag, Berlin Heidelberg, 1988.

[19] C. Bourlier, C. Le Bastard, V. Baltzart, Generalization of PILE method to the EM scattering from stratified subsurface with rough interlayers: application to the detection of debondings within pavement structure, IEEE Trans. Geosci. Rem. Sens. 53 (7) (July 2015) 4104–4115.

[20] N. Pinel, C. Le Bastard, M. Sun, Asymptotic modeling of coherent scattering form random rough layers: application to road survey by gpr at nadir, Int. J. Antenn. Propag. 2012 (2012) 874840.

[21] O. Glushko, R. Meisels, F. Kuchar, R. Danzer, Numerical and experimental investigations of surface roughness in 1d photonic crystals, J. Phys. Condens. Matter 20 (45) (oct 2008), 454220.

[22] A. Tabatabaeenejad, X. Duan, M. Moghaddam, Coherent scattering of electromagnetic waves from two-layer rough surfaces within the Kirchhoff regime, IEEE Trans. Geosci. Rem. Sens. 51 (7) (July 2013) 3943–3953.

[23] Karlene Rosera Maskaly, Garry R. Maskaly, W. Craig Carter, James L. Maxwell, Diminished normal reflectivity of one-dimensional photonic crystals due to dielectric interfacial roughness, Opt. Lett. 29 (23) (Dec 2004) 2791–2793.

[24] Karlene Rosera Maskaly, W. Craig Carter, Richard D. Averitt, James L. Maxwell, Application of the homogenization approximation to rough one-dimensional photonic crystals, Opt. Lett. 30 (21) (Nov 2005) 2930–2932.

[25] Alma K. González-Alcalde, Eugenio R. Méndez, Emiliano Terán, L. Fabio, S. Cuppo, J.A. Olivares, Augusto García-Valenzuela, Reflection of diffuse light from dielectric one-dimensional rough surfaces, J. Opt. Soc. Am. A 33 (3) (Mar 2016) 373–382.

[26] J.A. Ogilvy, Wave scattering from rough surfaces, Rep. Prog. Phys. 50 (1987) 1553–1608.

[27] A.G. Voronovich, Wave Scattering from Rough Surfaces, Volume 17 of *Wave Phenomena*, second ed., Springer-Verlag, Berlin, 1998.

[28] I.A. Lujan-Cabrera, C.F. Ramirez-Gutierrez, J.D. Castaño-Yepes, M.E. Rodriguez-Garcia, Effects of the interface roughness in the optical response of one-dimensional photonic crystals of porous silicon, Phys. B Condens. Matter 560 (2019) 133–139.

[29] M. Born, E. Wolf, Principles of Optics, seven edition, Cambridge University Press, 1999.

[30] Tanos Mikhael Elfouhaily, Charles-Antoine Guérin, A critical survey of approximate scattering wave theories from random rough surfaces, Waves Random Media 14 (4) (2004) R1–R40.

[31] A.G. Voronovich, The Kirchhoff and related approximations, in: Alexei A. Maradudin (Ed.), *Light Scattering And Nanoscale Surface Roughness*, Nanostructure Science and Technology, Chapter 2, Springer, New York, USA, 2007, p. 35.

[32] J.A. Sánchez-Gil, A.A. Maradudin, E.R. Méndez, Limits of validity of three perturbation theories of the specular scattering of light from one-dimensional, randomly rough, dielectric surfaces, J. Opt. Soc. Am. A 12 (7) (Jul 1995) 1547–1558.

[33] M. Franco, M. Barber, M. Maas, O. Bruno, F. Grings, E. Calzetta, Validity of the Kirchhoff approximation for the scattering of electromagnetic waves from dielectric, doubly periodic surfaces, J. Opt. Soc. Am. A 34 (12) (Dec 2017) 2266–2277.

[34] first ed., in: Dusan Losic, Abel Santos (Eds.), Nanoporous Alumina, vol. 219, Springer International Publishing, Switzerland, 2015.

[35] Yuting Chen, Abel Santos, Ye Wang, Tushar Kumeria, Junsheng Li, Changhai Wang, Dusan Losic, Biomimetic nanoporous anodic alumina distributed bragg reflectors in the form of films and microsized particles for sensing

applications, ACS Appl. Mater. Interfaces 7 (35) (2015) 19816–19824. PMID: 26287736.

[36] Santos Abel, Tushar Kumeria, Dusan Losic, Nanoporous anodic alumina: a versatile platform for optical biosensors, Materials 7 (6) (2014) 4297–4320.

[37] E. Calvo, M. L. Martínez Ricci, L. Missoni, and F. Ojeda. Patente Internacional (Pct/ib2016/054327): Method for Structural Colouration of Anodised Aluminium by Forming Photonic Cristals by Means of Current Pulses.

[38] Yuting Chen, Abel Santos, Ye Wang, Tushar Kumeria, Changhai Wang, Junsheng Li, Dusan Losic, Interferometric nanoporous anodic alumina photonic coatings for optical sensing, Nanoscale 7 (2015) 7770–7779.

[39] W. Luis Mochán, Marcelo del Castillo-Mussot, Rubén G. Barrera, Effect of plasma waves on the optical properties of metal-insulator superlattices, Phys. Rev. B 35 (Jan 1987) 1088–1098.

[40] Pochi Yeh, Optical Waves in Layered Media. Wiley Series in Pure and Applied Optics, Wiley, Hoboken, New Jersey, USA, 2005.

[41] J.S. Pérez-Huerta, D. Ariza-Flores, R. Castro-García, W.L. Mochán, G.P. Ortiz, V. Agarwal, Reflectivity of 1d photonic crystals: a comparison of computational schemes with experimental results, Int. J. Mod. Phys. B 32 (11) (2018), 1850136.

[42] Carl Eckart, The scattering of sound from sea surface, J. Acoust. Soc. Am. 25 (3) (1953) 566–570.

[43] E. Hecht, A. Zajac, Optica, Addison-Wesley Iberoamericana, S.A., 1986.

[44] L.A. Dorado, R.A. Depine, Modeling of disorder effects and optical extinction in three-dimensional photonic crystals, Phys. Rev. B 79 (2009), 045124.

[45] K. Glazebrook, J. Brinchmann, J. Cerney, C. DeForest, D. Hunt, T. Jenness, T. Luka, R. Schwebel, C. Soeller, Pdl: the perl Data Language v.2.4.4, Dr. Dobb's J. 5 (5) (1997). http://pdl.perl.org.

[46] Caroline A. Schneider, Wayne S. Rasband, Kevin W. Eliceiri, Nih image to imagej: 25 years of image analysis, Nat. Methods 9 (7) (2012) 671–675.

[47] Guillermo P. Ortiz, W Luis Mochán, Keller's theorem revisited, New J. Phys. 20 (2) (feb 2018), 023028.

[48] E.D. Palik (Ed.), Handbook of Optical Constants of Solids, Academic press handbook series. Academic, Orlando, Florida, 1985.

[49] Mikhail N. Polyanskiy. Refractive Index Database.

[50] F. James, MINUIT Function Minimization and Error Analysis: Reference Manual Version 94.1, 1994.

[51] http://www.metalium.mx/aluminio/aluminio-1100/1100.

[52] V.J. Toranzos, G.P. Ortiz, A.J. Busso, R.R. Koropecki, Propiedades ópticas *in situ* de capas múltiples nanoestructuradas, ANALES AFA 20 (2008) 65–68.

[53] J. Victor, Toranzos. *Electroluminiscencia en Silicio Poroso Nanoestructurado*, PhD thesis, Universidad Nacional de Salta, 2014.